# Multisensor Image Fusion Using a Pulse Coupled Neural Network

Yi Zheng[1] and Ping Zheng[2]

[1] School of Information and Electronic Engineering, Shandong Institute of Business and Technology, 264005 Yantai, China
zhengyi@sdibt.edu.cn
[2] Institute for Pattern Recognition and Artificial Intelligence, Huazhong University of Science and Technology, 430074 Wuhan, China
pzhhust@sohu.com

**Abstract.** Multisensor image fusion has its effective utilization for surveillance. In this paper, we utilize a pulse coupled neural network method to merge images from different sensors, in order to enhance visualization for surveillance. On the basis of standard mathematical model of pulse coupled neural network, a novel step function is adopted to generate pulses. Subjective and objective image fusion performance measures are introduced to assess the performance of image fusion schemes. Experimental results show that the image fusion method using pulse coupled neural network is effective to merge images from different sensors.

**Keywords:** image fusion, pulse coupled neural network, step function, performance assessment.

## 1 Introduction

Surveillance systems are currently being used for security surveillance, navigation as well as battlefield monitoring. The purpose of image fusion is to extract and synthesize information from multiple images in order to produce a more accurate, complete and reliable composite image of the same scene or target, so that the fused image is more suitable for human or machine interpretation. In this way, surveillance systems utilize the synergism of different unmated imaging sensors, such as a CCD camera and an infrared camera. In this paper, we consider a more restricted case of the multisensor fusion problem, i.e. we explore only the case of merging registered image pairs. And image fusion algorithms discussed in this paper are pixel-level.

A pulse coupled neural network (abbr. PCNN) is a biological inspired neural network developed by Eckhorn in 1990 and based on experimental observations of synchronous pulse bursts in cat visual cortex[1]. It is characterized by the global coupling and pulse synchronization of neurons. PCNN is different from what we generally mean by artificial neural networks in the sense that it does not train. PCNN is quite powerful and there are extensive image processing applications, such as segmentation, edge extraction, noise suppression, motion processing, and so on[2].

F.L. Wang et al. (Eds.): AICI 2010, Part I, LNAI 6319, pp. 79–87, 2010.

PCNN has a history of some two decades but has solid applications in the field of image fusion only in the past ten years[3-9]. And it is still in underdevelopment stage and shows tremendous promise. In this paper, we explore characters of PCNN and utilize the PCNN model to perform image fusion in terms of gray level values.

The paper is organized as follows. In Section 2, we will illustrate the structure of PCNN in image fusion, enumerate the mathematical model of PCNN, and modify its step function of the mathematical model. The experiments are presented in Section 3. In the last section, some concluding remarks and future directions for study are given.

## 2 Image Fusion Based on PCNN

### 2.1 Structure of PCNN in Image Fusion

In a pulse coupled neural network, each neuron consists of three parts: the receptive field, the modulation field and the pulse generator. The simplified model of a PCNN neuron is shown in Fig. 1[10].

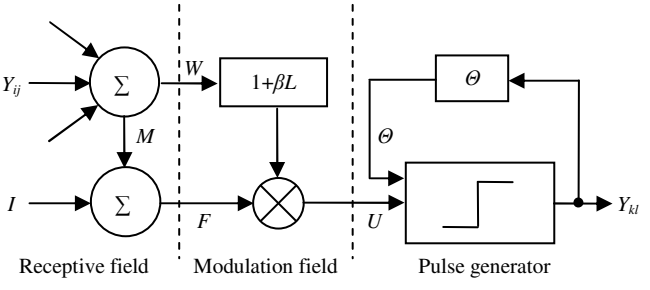


**Fig. 1.** Simplified model of a PCNN neuron

In Fig. 1, $I$, $U$, $L$, $\beta$ is the external stimulus, the interior action, the linking input and the linking strength, respectively. $F$ is the feeding part, which includes the input from both exterior and other neurons. PCNN is a feeding back network. $Y_{ij}$ is the input from other neurons, and $Y_{kl}$ is the output to other neurons. $\Theta$ is the variable threshold function. $M$ and $W$ are the matrix of linking weights of the feedback path and link path respectively.

Fig. 2 shows the connection model of a single neuron within the PCNN. PCNN is a single layer of pulse coupled neurons, and each neuron is corresponding to an input image pixel and an output image pixel.

When a pulse coupled neural network is applied to two dimensional image fusion, the image matrix corresponds to the neural network composed of $P \times Q$ PCNN neurons. And the gray level value of each pixel corresponds to the input of each neuron $I$. Each PCNN neuron receives inputs from its own stimulus and also from neighboring sources, i.e. outputs of other PCNN neurons in feeding radius is added to the input.

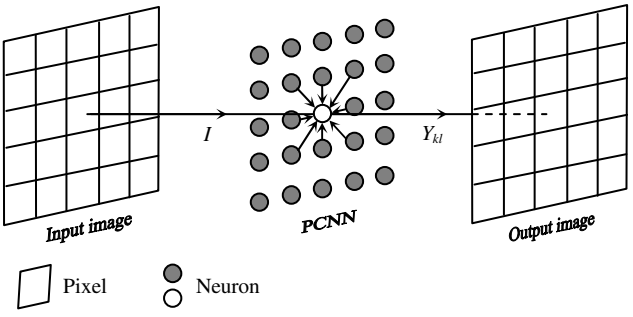


**Fig. 2.** Connection model of a PCNN neuron

### 2.2 Mathematical Model of PCNN

The multi-spectral PCNN is a set of parallel PCNNs each operating on a separate channel of the input with both inter- and intra-channel linking. In the surveillance system, input image pairs are visible and infrared images. Thus the number of channel is 2. Discrete equations of each neuron are the following.

$$F_{ij}(n) = e^{-\alpha_F} F_{ij}(n-1) + V_F \sum_{kl} M_{ijkl} Y_{kl}(n-1) + I_{ij} \tag{1}$$

$$L_{ij}(n) = e^{-\alpha_L} L_{ij}(n-1) + V_L \sum_{kl} W_{ijkl} Y_{kl}(n-1) \tag{2}$$

$$U_{ij}(n) = F_{ij}(n)\left(1 + \beta L_{ij}(n)\right) \tag{3}$$

$$Y_{ij}(n) = \begin{cases} 1, & \text{if } U_{ij}(n) > \Theta_{ij}(n-1) \\ 0, & \text{otherwise} \end{cases} \tag{4}$$

$$\Theta_{ij}(n) = e^{-\alpha_\Theta} \Theta_{ij}(n-1) + V_\Theta Y_{ij}(n) \tag{5}$$

Equation (1), (2) and (3) are the mathematical models of the feeding input unit, linking input unit and modulating coupler respectively. Equation (4) and (5) are the expression of the step function and variable threshold function of the pulse generator respectively. Among these equations above, $i$ and $j$ correspond to the location of a neuron in the layer of PCNN, $k$ and $l$ also do.

Parameters denoted in the mathematical models are identical to ones denoted in Fig. 1. $M/V_F$ and $W/V_L$ are the matrix of linking weights/magnitude scaling coefficients of the feedback path and link path respectively. $M$ and $W$ are traditionally local and Gaussian. $\Theta$ and $V_\Theta$ are the output of variable threshold function and the magnitude scaling coefficient for dynamic threshold respectively. $V_\Theta$ is a large constant that is generally more than an order of magnitude greater than the average of $U$. $U$ is the internal state of the neuron, which will be compared with the dynamic

threshold $\Theta$ to produce the output $Y$, as shown in (4). Each neuron has the same linking strength $\beta$ in these five equations.

Initially, values of arrays, $F$, $L$, $U$, and $Y$ are all set to zero. The values of the $\Theta$ element are initially 0 or some larger value depending on our needs. In the proposed image fusion method using PCNN, the values of the $\Theta$ elements are all set to be 0 initially.

### 2.3 Improved PCNN Model

In Eckhorn's PCNN model, the pulse generator is a step function. In the proposed image fusion method using PCNN, the improved PCNN model is adopted[5, 11]. Equation (4) can be replaced by a novel step function related to the dynamic threshold $\Theta_{ij}$, as shown in (6).

$$Y_{ij}(n) = \begin{cases} \Theta_{ij}(n-1), & \text{if } U_{ij}(n) > \Theta_{ij}(n-1) \\ 0, & \text{otherwise} \end{cases} \tag{6}$$

The threshold of each PCNN neuron can represent approximately the fire time of the corresponding neuron. A fire mapping image can be obtained by mapping the output threshold of each neuron to the gray level scope of the corresponding image.

The gray level value of the fused image is expressed by the times the neuron fires. Each neuron that has any stimulus will fire in the initial iteration in turn, which will create a large threshold value. It will then take several iterations before the threshold values decay enough to allow the neuron to fire again. It tends to circumvent these initial iterations which contain little information.

## 3 Experimental Results

In this section, the performance of the proposed image fusion method using PCNN is tested and compared with those of some conventional image fusion schemes using subjective and objective image fusion performance measures. Input image pairs used in the experiments are downloaded from [12]. These image pairs are registered and with 256 gray levels.

In the experiments, we use three image fusion schemes for comparison, i.e. Principle Component Analysis (abbr. PCA) based image fusion[13], Contrast pyramid based image fusion[14] and Discrete Wavelet Transform (abbr. DWT) based image fusion[15]. In DWT based image fusion scheme, the wavelet decomposition level is 4 and 'symlet 4' are used as wavelets which are compactly supported wavelets and nearly symmetric with highest number of vanishing moments for a given supporting width. The proposed image fusion method using PCNN requires no training. Partial PCNN parameter values used in the experiments are listed as follows[16]:

PCNN iteration time $n = 30$
Delay factor for linking $\alpha_L = 1.0$
Delay factor for dynamic threshold $\alpha_\Theta = 0.012$
Magnitude scaling coefficient of link path $V_L = 0.2$
Magnitude scaling coefficient for dynamic threshold $V_\Theta = 40$

The linking strength $\beta$ plays an important role in the image fusion method based on PCNN. For a two-channel image fusion method, the value of $\beta$ for visible image channel is equal to the value of $\beta$ for infrared image channel. In the succedent experiments, $\beta$ is set to be 0.5.

Both $M$ and $W$, the matrix of linking weights of the feedback path and link path, are usually symmetrical, and determined by specific applications.

A pair of images is shown in Fig. 3. The image shown in Fig. 3(a) is the visible image, and the image shown in Fig. 3(b) is the infrared image. The important features of the image pair in Fig. 3 are man and trees.

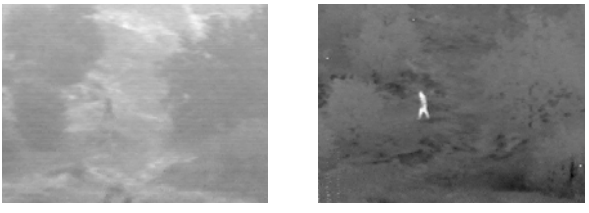

(a) (b)

**Fig. 3.** Trees.bmp (a) visible image; (b) infrared image

Fused images using different schemes are illustrated respectively in Fig. 4.

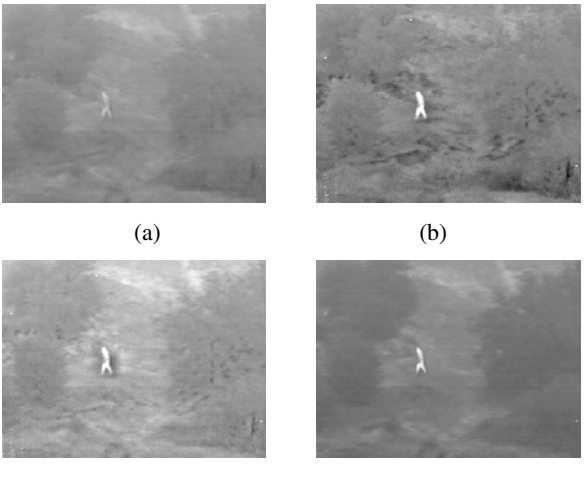

(a) (b)

(c) (d)

**Fig. 4.** Fused images of Trees.bmp (a) PCA; (b) Contrast pyramid; (c) DWT; (d) PCNN

In this experiment, the result of PCA based image fusion algorithm is not very impressive and the outline of the man is blurred to the surroundings. Results of other schemes are as obvious and well-marked as ones in the infrared image. Features both in the visible image and in the infrared one, such as man, trees and middle area, are merged commendably in Fig. 4(d).

Subjective and perceptive comparisons are shown hereinbefore. Then four objective image fusion performance measures are introduced to assess these schemes, i.e. entropy, variance, the fusion performance metric proposed by Xydeas and Petrovic[17, 18] and the fusion performance metric proposed by Piella and Heijmans[19]. These four measures do not require a ground truth or a reference image.

Entropy of an image is a measure of information content[20]. It is the average number of nits needed to quantize the intensities in the image. The more entropy of an image, the more information content is included in the image. It is defined as

$$H = -\sum_{g=0}^{L-1} p(g) \cdot \log_2 p(g) \tag{7}$$

where $p(g)$ is the probability of gray level $g$, the range of $g$ is [0, …, $L$-1], and $\sum_{g=0}^{L-1} p(g) = 1$. $L$ is equal to 256 for a gray level image.

Variance, another name for the second moment, measures the gray-level contrast used to establish the relative smoothness[21]. Variance of the image is defined as

$$\sigma^2 = \sum_{g=0}^{L-1} (g - \overline{g})^2 \cdot p(g) \tag{8}$$

where $\overline{g}$ is the statistical mean of gray levels, and it is defined as

$$\overline{g} = \sum_{g=0}^{L-1} g \cdot p(g) \tag{9}$$

The greater variance of an image, the greater gray-level contrast.

The metric proposed by Xydeas and Petrovic can measure the amount of edge information transferred from the source images to the fused image to give an estimation of the performance of fusion algorithms. It uses a Sobel edge operator to calculate the strength and orientation information of each pixel in the source and fused images. Thus overall edge strength and orientation preservation values can be obtained. It is the normalized weighted edge information preservation values $Q^{AB/F}$ that we use to evaluate and compare performance of image fusion algorithms. This performance score falls to the range 0 to 1, with 0 representing total loss of input information and 1 ideal fusion.

The metric proposed by Piella and Heijmans is based on an image quality metric introduced in [22]. In the method, the important edge information of human visual system is taken into account to evaluate the relative amount of salient information contained in each of the input images that has been transferred into the fused image without introducing distortions. The edge-dependent fusion quality index $Q_E$ is calculated with $\alpha = 1$. Similar to $Q^{AB/F}$, this performance score varies from 0 to 1, with 0 representing total loss of input edge information and 1 ideal fusion.

It is noticeable that both Xydeas and Piella metrics are based on edges and consequently fused images containing some significant artifacts can sometimes be inadvertently rated high by the metrics but look inferior perceptually.

Objective performance assessments of these schemes are shown in Table 1.

**Table 1.** Performance assessments of image fusion schemes (Trees.bmp)

| | PCA | Contrast pyramid | DWT | PCNN |
|---|---|---|---|---|
| Entropy | 5.93 | 6.18 | 6.32 | 5.72 |
| Variance | 232.4 | 350.2 | 435.1 | 231.2 |
| $Q^{AB/F}$ | 0.39 | 0.52 | 0.43 | 0.52 |
| $Q_E$ | 0.72 | 0.73 | 0.70 | 0.76 |

Of all these four image fusion schemes here, $Q^{AB/F}$ and $Q_E$ of the image fused by the PCNN method are the greatest. However, other two objective image fusion performance measures of the PCNN method, such as entropy and variance, are the least than those of other three schemes.

Another pair of images is shown in Fig. 5. The image shown in Fig. 5(a) is the visible image, and the image shown in Fig. 5(b) is the infrared image. The salient features of the image pair in Fig. 5 are man, road and dunes.

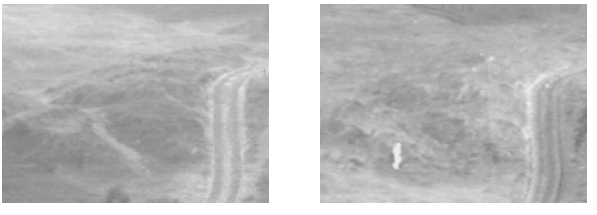

(a) (b)

**Fig. 5.** Dune.bmp (a) visible image; (b) infrared image

Fused images using different schemes are illustrated respectively in Fig. 6.

In Fig. 6(a), the man is as inconspicuous as in the visible image, despite dunes are clear. The experimental result of PCA based image fusion algorithm shows that it is disabled to fuse the image pair. Except for PCA based image fusion algorithm, other three schemes are effective to merge the visible image and the infrared one. Dunes and the man are clear in the image fused by the PCNN method. It is observable that shapes of dunes are unclear in Fig. 6(c).

Objective performance assessments of these schemes are shown in Table 2.

Of all these four image fusion schemes here, four objective image fusion performance measures of the PCNN method are the greatest in Table 2. These performance assessments of the PCNN method are satisfying.

These four schemes can more or less preserve the salient information and enhance the contrast for visualization. Subjective and objective evaluations show that the PCNN method is effective as a whole.

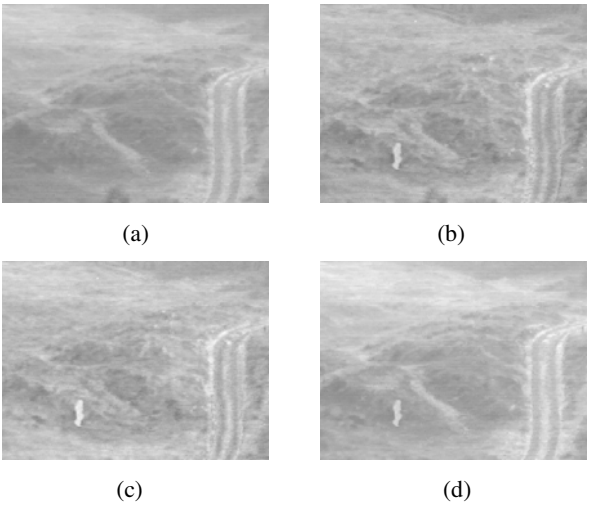

(a) (b)

(c) (d)

**Fig. 6.** Fused images of Dune.bmp (a) PCA; (b) Contrast pyramid; (c) DWT; (d) PCNN

**Table 2.** Performance assessments of image fusion schemes (Dune.bmp)

| | PCA | Contrast pyramid | DWT | PCNN |
|---|---|---|---|---|
| Entropy | 6.23 | 6.06 | 6.12 | 6.30 |
| Variance | 370.3 | 266.4 | 288.3 | 435.9 |
| $Q^{AB/F}$ | 0.57 | 0.50 | 0.46 | 0.60 |
| $Q_E$ | 0.80 | 0.75 | 0.73 | 0.82 |

## 4 Conclusions

In this paper, the image fusion method using PCNN for surveillance is studied. The simplified model and connection model of PCNN neuron are illustrated and the image fusion method using PCNN is presented. The PCNN method is compared with other three image fusion algorithms through some subjective and objective image fusion performance measures. Experimental results show that the PCNN method is effective to merge visible and infrared images from different sensors. Future work will concentrate on a study of automatic determination of PCNN parameters. In addition, because of parallel computation performance of PCNN, a challenging direction for future work could be the extension of the image fusion method using PCNN to the case of real-time image fusion of visible and infrared videos for automatic navigation.

## References

1. Eckhorn, R., Reitboeck, H.J., Arndt, M., Dicke, P.: Feature Linking via Synchronization among Distributed Assemblies: Simulation of Results from Cat Cortex. Neural Computation 2, 293–307 (1990)
2. Lindblad, T., Kinser, J.M.: Image Processing Using Pulse-coupled Neural Networks, 2nd edn. Springer, Netherlands (2005)

3. Broussard, R.P., Rogers, S.K., Oxley, M.E., Tarr, G.L.: Physiologically Motivated Image Fusion for Object Detection Using a Pulse Coupled Neural Network. IEEE Transactions on Neural Networks 10, 554–563 (1999)
4. Xu, B., Chen, Z.: A Multisensor Image Fusion Algorithm Based on PCNN. In: Proceedings of the Fifth World Congress on Intelligent Control and Automation, vol. 4, pp. 3679–3682 (2004)
5. Miao, Q., Wang, B.: A Novel Adaptive Multi-focus Image Fusion Algorithm Based on PCNN and Sharpness. In: Proceedings of SPIE, vol. 5778, pp. 704–712 (2005)
6. Wang, Z., Ma, Y.: Dual-channel PCNN and Its Application in the Field of Image Fusion. In: Third International Conference on Natural Computation, vol. 1, pp. 755–759 (2007)
7. Huang, W., Jing, Z.: Multi-focus Image Fusion Using Pulse Coupled Neural Network. Pattern Recognition Letters 28, 1123–1132 (2007)
8. Qu, X.-b., Yan, J.-w., Xiao, H.-z., Zhu, Z.-q.: Image Fusion Algorithm Based on Spatial Frequency-motivated Pulse Coupled Neural Networks in Nonsubsampled Contourlet Transform Domain. Acta Automatica Sinica 34, 1508–1514 (2008)
9. Wang, Z., Ma, Y., Gu, J.: Multi-focus Image Fusion Using PCNN. Pattern Recognition 43, 2003–2016 (2010)
10. Ranganath, H.S., Kuntimad, G.: Iterative Segmentation Using Pulse Coupled Neural Networks. In: Proceedings of SPIE, vol. 2760, pp. 543–554 (1996)
11. Shi, M.-h., Zhang, J.-y., Zhu, X.-j., Zhang, X.-b.: A Method of Image Gauss Noise Filtering Based on PCNN. Computer Applications 22, 1–4 (2002) (in Chinese)
12. Toet, A.: `http://www.imagefusion.org/images/toet2`
13. Chavez Jr., P.S., Sides, S.C., Anderson, J.A.: Comparison of Three Different Methods to Merge Multiresolution and Multispectral Data: Landsat TM and SPOT Panchromatic. Photogrammetric Engineering and Remote Sensing 57, 295–303 (1991)
14. Toet, A., van Ruyven, L.J., Valeton, J.M.: Merging Thermal and Visual Images by a Contrast Pyramid. Optical Engineering 28, 789–792 (1989)
15. Li, H., Manjunath, B.S., Mitra, S.K.: Multisensor Image Fusion Using the Wavelet Transform. Graphical Models and Image Processing 57, 235–245 (1995)
16. Johnson, J.L., Padgett, M.L.: PCNN Models and Applications. IEEE Transactions on Neural Networks 10, 480–498 (1999)
17. Xydeas, C.S., Petrovic, V.: Objective Image Fusion Performance Measure. Electronics Letters 36, 308–309 (2000)
18. Xydeas, C., Petrovic, V.: Objective Pixel-level Image Fusion Performance Measure. In: Proceedings of SPIE, vol. 4051, pp. 89–98 (2000)
19. Piella, G., Heijmans, H.: A New Quality Metric for Image Fusion. In: 2003 International Conference on Image Processing, vol. 3, pp. III-173–III-176 (2003)
20. Hu, L.-m., Gao, J., He, K.-f.: Research on Quality Measures for Image Fusion. Acta Electronica Sinica 32, 218–221 (2004) (in Chinese)
21. Singh, H., Raj, J., Kaur, G., Meitzler, T.: Image Fusion Using Fuzzy Logic and Applications. In: IEEE International Conference on Fuzzy Systems, vol. 1, pp. 337–340 (2004)
22. Wang, Z., Bovik, A.C.: A Universal Image Quality Index. IEEE Signal Processing Letters 9, 81–84 (2002)